Desalination and Water Treatment
www.deswater.com

doi: 10.1080/19443994.2015.1027964

57 (2016) 9272–9285
April

Taylor & Francis
Taylor & Francis Group

A random forest approach for predicting the removal of Congo red from aqueous solutions by adsorption onto tin sulfide nanoparticles loaded on activated carbon

Nahid Dehghanian[a], Mehrorang Ghaedi[b,*], Amin Ansari[a], Abdolmohammad Ghaedi[c], A. Vafaei[c], M. Asif[d], Shilpi Agarwal[e], Inderjeet Tyagi[e], Vinod Kumar Gupta[e,f,*,1]

[a]*Department of Chemistry, Science and Research Branch, Islamic Azad University, Fars, Iran, emails: n.dehghanian2013@gmail.com (N. Dehghanian), nimaansari1132@gmail.com (A. Ansari)*
[b]*Chemistry Department, Yasouj University, Yasouj 75918-74831, Iran, email: m_ghaedi@mail.yu.ac.ir*
[c]*Faculty of Science, Department of Chemistry, Gachsaran Branch, Islamic Azad University, P.O. Box 75818-63876, Gachsaran, Iran, emails: abm_ghaedi@yahoo.com (A. Ghaedi), azam_vafaei86@yahoo.com (A. Vafaei)*
[d]*Chemical Engineering Department, King Saud University, Riyadh, Saudi Arabia, email: masif@ksu.edu.sa*
[e]*Department of Chemistry, Indian Institute of Technology Rookree, Roorkee 247667, India, Tel. +91 1332285801; Fax: +91 1332273560; emails: shilpi.agarwal2307@gmail.com (S. Agarwal), indertyagi011@gmail.com (I. Tyagi), vinodfcy@iitr.ac.in, vinodfcy@gmail.com (V.K. Gupta)*
[f]*Center for Environment and Water, The Research Institute, King Fahd University of Petroleum and Minerals, Dhahran, Saudi Arabia*

Received 22 December 2014; Accepted 5 March 2015

ABSTRACT

In this work, tin sulfide nanoparticles loaded on activated carbon (SnS-NP-AC) was synthesized and characterized using various analytical techniques, such as SEM, BET, XRD, and UV–Vis spectroscopy. The impact of influential parameters such as the contact time, adsorbent dosage, pH, and initial dye concentration was investigated and optimization was carried out using random forest model. The optimized values of influential parameters i.e. pH, contact time, adsorbent dosage, and initial dye concentration were found to be 1, 4 min, 0.03 g, and 15 mg L^{-1}, respectively. At these optimized values CR achieve highest removal percentage (99%) and maximum adsorption capacity (384.6 mg g^{-1}). The experimental equilibrium data were fitted to different adsorption isotherm models i.e. Langmuir, Freundlich, Tempkin, and Dubinin–Radushkevich, among them the Langmuir model is found to be the best fitted and well suited model for evaluating and analyzing the actual behavior of adsorption process. The Kinetic experimental data were well fitted and they are in good agreement with pseudo-second-order and intraparticle diffusion model.

Keywords: Adsorption; Tin sulfide nanoparticles; Activated carbon; Random forest; Congo red

*Corresponding authors.

[1]Department of Applied Chemistry, University of Johannesburg, Johannesburg, South Africa.

1. Introduction

In recent years, the trend of several computational techniques for solving problem in the field of science and engineering has been dramatically increased. Soft computing technique is a very broad term, which covers approaches to model, design, and optimization, of various systems without applying mathematical models. An accurate and effective soft computing technique can be designed based on the prevailing problems to be solved. Soft computing techniques classically involve many fields, including artificial neural networks, fuzzy inference system, adaptive neuro-fuzzy inference system, support vector machine, random forest (RF), firefly algorithm, particle swarm optimization (PSO), imperialist competitive algorithm and genetic algorithm, and their hybrids and derivatives [1–10]. RF is one of the novel and powerful technique model, which was used to predict the retention indices of some polycyclic aromatic hydrocarbons [11], selected subsets of the metabolites and transcripts, which show association with potato tuber flesh color and enzymatic discoloration [12] prediction of N_2O emission from local information [13] variable selection and a regression method for predicting wetland biomass [14] predict outcomes of intramuscular PSO as lengthening [15] predicting the presence of *Echinococcus multiloculars* in the intermediate host *Ochotona* spp. and removal of bromophenol blue using activated carbon (AC) obtained from *Astragalus bisulcatus* tree [2].

Dyes are extensively used in various industrial activities including coloring, paper, textiles, plastics, leather, cosmetics, and food. Because of their complex (aromatic) molecular structures dyes are stable towards heat and oxidizing agent, and are mainly non-biodegradable. Additionally, to their non-biodegradable nature, most dyes are noxious and harmful to several micro-organisms as it directly destroys or inhibit their catalytic activities [16]. The toxicity of dyes on plant, animal, and human health is well known. Among, various classification of dyes (cationic, anionic, and neutral), the cationic ones are more toxic [17]. On the other hand, the azo dyes containing reactive groups viz. oxygen, nitrogen, and sulfur due to the presence of more reactive groups in their structure are capable of forming covalent bond with other species through oxygen, nitrogen, or sulfur atoms of cellulose (hydroxyl group), protein (amino, hydroxyl, and mercaptan groups), and polyamides (amino group) compounds [18]. Hence, the rapid removal of noxious dyes from waste effluents of aquatic source is a challenging requirement. Due to their synthetic aromatic structure and hazardous nature, the wastewater treatment is a difficult and expensive task. Diverse chemical and physical treatment procedures, such as ozonation, membrane separation, and adsorption, have been applied. Among them, adsorption-based procedure due to unique advantages, such as adsorbents versatility, non-toxicity, high adsorption capacity, and cost-effective and high removal percentage in addition to regeneration ability of adsorbent is a most effective technique [19]. The adsorption technique is based on the transfer of pollutants from the solution to the solid phase, and it is superior to other conventional dye removal techniques in terms of initial cost, simplicity of design, ease of operation, and non-toxicity of the utilized adsorbents compared with other conventional wastewater treatment methods [20,21]. AC solely as adsorbent, although, has advantages such as low cost and non-toxic nature, but has low adsorption capacity [22]. Due to the presence of porous carbon backbone, it is easy for AC to be impregnated with various functional groups and hence proved to be a good prospective material with enhanced adsorption capacity by the efficient increase in reactive center and surface area.

Nanoparticles exhibit intrinsic surface activity and due to their large surface areas and active sites or functional group, they strongly chemisorb many perilous chemical compounds. The SnS-NPs are widely utilized as photosensitive material and catalysts, and applied widely as in chemical analysis due to their high electrical conductivity and optical properties.

In this work, the SnS-NP-AC was synthesized and characterized using SEM, BET, X-ray diffraction (XRD), and UV–Vis analysis. The impact of effective parameters such as the contact time, adsorbent dosage, pH, and initial dye concentration was investigated and optimized using RF model. The treatment of polluted water with SnS-NP-AC causes the removal of high amount of noxious CR in a very short period of time.

2. Experimental

2.1. Instruments and reagents

All chemicals including Congo red (Molecular Formula: $C_{32}H_{22}N_6Na_2O_6S_2$, Molecular Weight: 696.663219 g/mol) IUPAC Name (disodium;4-amino-3-[[4-[4-[(1-amino-4-sulfonatonaphthalen-2-yl)diazenyl] phenyl]phenyl]diazenyl]naphthalene-1-sulfonate) Fig. 1, tin acetate, thioacetamide, AC, NaOH, and HCl with the highest purity available were purchased from Merck Co. (Darmstadt, Germany). The stock solution (200 mg L^{-1}) of CR was prepared by dissolving 20 mg of solid dye in 100 mL double distilled water and the working concentrations were prepared by their suitable dilution.

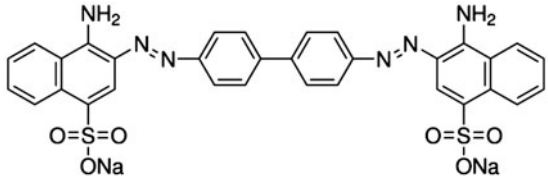

Fig. 1. The structure of Congo red.

The pH measurements were carried out using pH/Ion meter model-691 (Metrohm, Switzerland).

2.2. Measurements of dye uptake

The dye concentrations were determined according to general traditional photometry method at maximum wavelength over working concentration. The efficiency of CR removal was determined at different time intervals (in the range of 0.5–5 min) and the equilibrium was established after 4 min of contact time. The effect of initial pH on the removal of CR was evaluated in the pH range of 1–6, by contacting 50 mL of 10 mg L^{-1} of initial dye concentration with 0.01, 0.02, and 0.03 g of SnS-NP-AC for 4 min of contact time. The experiments were also performed in the initial CR concentration range of 5–70 mg L^{-1} to obtain adsorption isotherms. The CR removal percentage was calculated using the following equation:

$$\%\ \text{CR removal} = ((C_0 - C_t)/C_0) \times 100 \quad (1)$$

where C_0 (mg L^{-1}) and C_t (mg L^{-1}) are the concentrations of target at initial and after time t, respectively. The adsorbed CR amount (q_e (mg g^{-1})) was calculated by the following mass balance relationship:

$$q_e = (C_0 - C_e)\ V/W \quad (2)$$

where C_0 and C_e (mg L^{-1}) are the initial and equilibrium dye concentrations in aqueous solution, respectively, V (L) is the volume of the solution, and W (g) is the mass of the adsorbent.

2.3. Random forest

RF is an ensemble machine learning technique introduced by Breiman based on a combination of a large set of classification and regression trees method [23]. RF algorithms are recursively employed to create multiple decision trees, until a maximal tree is generated. Since, a very large tree might over fit the new data; a pruning algorithm is used to select an optimal tree structure. Finally, average individual tree predictions across the entire forest are generated. The RF model is a collection of many un-pruned regression trees. Each tree is grown based on a bootstrap replicate of the training data. To construct a tree, at each iteration, two-third of the initial sample to train the RF sample (called the in-bag samples) is employed, while the remaining third, the "out of bag" (OOB) initial samples, are retained for testing the prediction error of the RF. Each tree is grown to the largest extent possible, and then predictions are constructed by averaging all the tree outputs. Since the OOB data are not employed in the making of each tree; therefore, it is regarded as a test set to get a running unbiased estimate of the prediction error and variable importance as trees are added to the forest. The OOB error estimate is an unbiased estimate of the generalization error, and this is almost same to that obtained by cross-validation.

The RF algorithm has several tuning parameters, such as n_{tree} (the number of regression trees grown based on a bootstrap sample of the original data-set, the default value is 500 trees); m_{try} (the number of various predictors to try at each node, the default value is one third of the total number of the variables); and node size (minimum size of terminal nodes). Larger number of node size led to smaller trees (the default values are 1 and 5 for classification and regression, respectively). In practice, the number of trees (n_{tree}) and the size of the variable subset (m_{try}) in the RF modeling are the two key user-defined parameters that should be optimized to reach the ideal model by minimizing the OOB error.

The obtained experimental data are randomly divided into a training set and testing set. Among 33 data, 25 are considered as training data and 8 as testing data. The inputs consist of concentration (mg L^{-1}), amount of adsorbent (g), and contact time (min). The output obtained is in the form of the removal (%). Inputs and outputs are normalized between 0.1 and 0.9 to avoid numerical overflows due to very large or very small weights. The normalization equation employed is of the following:

$$y = (x_i - x_{min}/x_{max} - x_{min}) \times 0.8 + 0.1 \quad (3)$$

where y is the normalized value of x_i. The x_{max} and x_{min} are the maximum and minimum value of x_i, respectively. For the created model, two parameters are applied to test the performance of the RF models. The mean squared error (MSE) and the coefficient of determination (R^2), which can be indicated as follows:

$$\mathrm{MSE} = \frac{1}{N}\sum_{i=1}^{N}\left(\left|y_{\mathrm{prd},i} - y_{\mathrm{exp},i}\right|\right)^2 \quad (4)$$

$$R^2 = 1 - \frac{\sum_{i=1}^{N}\left(y_{\mathrm{prd},i} - y_{\mathrm{exp},i}\right)}{\sum_{i=1}^{N}\left(y_{\mathrm{prd},i} - y_m\right)} \quad (5)$$

where $y_{\mathrm{prd},i}$, $y_{\mathrm{exp},i}$, N, y_m, the predicted value by RF model, experimental value, number of data, and average of the experimental value, respectively.

2.4. Preparation of SnS-NP-AC

SnS nanoparticles synthesis was based on the reaction of tin acetate ($Sn(CH_3COO)_2$) with thioacetamide (CH_3CSNH_2) in oxygen free water under nitrogen atmosphere [19,20]. Then, 10 mL of thioacetamide solution (0.1 mol L^{-1}) was added into solution of Sn $(CH_3COO)_2$ and tri-sodium citrate at pH of 6.0 and mixed vigorously following dilution to 50 mL. The total amounts of tin acetate, thioacetamide, and tri-sodium citrate in the mixture were 0.5, 1, and 5 mmol, respectively, when the mixture is heated at 40°C it results in the slow formation and growth of citrate-stabilized SnS nanoparticles (milky white precipitate) and after 6 h at the same condition the color of the reaction solution became milky white mixed with light yellow precipitate that can be easily separated from the mixture by centrifuge and washed several times with ultrapure water and ethanol to remove the impurities and tri-sodium citrate. Addition and vigorous mixing of 500 mL of the dispersed SnS nanoparticles suspension (0.5 g L^{-1}) with 10 g AC under magnetic stirring for up to 12 h lead to its deposition on the AC surface, and the amount of non-loaded SnS nanoparticle in the filtrate solutions were analyzed using UV–vis spectrophotometry. The carbon-supported SnS nanoparticles were generally dried at 110°C in an oven for 10 h. A mortar was used to homogeneously ground the carbon-supported SnS nanoparticles powders.

3. Results and discussion

3.1. Adsorbent characterization

Absorption measurements of SnS-NP-AC solutions were carried out on a Perkin Elmer Lambda 25 spectrophotometer (Massachusetts, USA) using a quartz cell with an optical path of 1 cm. Absorption spectra up to 6 h shows well-resolved absorption maximum related to the first electronic transition that is attributed to its sufficiently narrow size distribution of the SnS nanoparticles and shifts to the shorter wavelengths with decreasing its size of the nanoparticles (the quantum effect) (Fig. 2). The absorption edge of SnS (290–320 nm) is in the range of 4.26–3.86 eV that was obtained according to the well-known following relation [24]:

$$(ah\upsilon)^2 = A\left(E_g - h\upsilon\right) \quad (6)$$

where E_g represents the band gap and A is a constant. Intercept of line achieved by tracing $(ah\upsilon)^2$ vs. energy $(h\upsilon)$ shows band gap value in the range of 4.26–3.86 eV. The significant difference between bulk and evaluated band gap of SnS (3.67 compared to 3.86–4.26 eV) shows the decrease in the size of SnS nanoparticle. XRD pattern was recorded by an automated Philips X'Pert X-ray diffractometer (Philips Analytical X-ray, Netherlands) at 40 kV and 30 mA for 2θ values over 10°–80°. The peaks around 28.56°, 47.43°, and 56.25° reveal its cubic lattice structure that are assigned to the planes (1 1 1), (2 2 0), and (3 1 1), respectively (cubic phase) Fig. 3(a) [25]. Any diffracted peaks concerned to SnO or $Sn(OH)_2$ in the XRD pattern were not observed.

The volume average hydrodynamic diameter for the SnS nanoparticles, which is determined by the laser light scattering, was found around 60 nm with narrow size distribution of 0.15 polydispersity (Fig. 3(b)). The surface morphological properties of the SnS NPs were investigated by field emission scanning electron microscope (FE-SEM, Hitachi S4160, Tokyo, Japan) under an acceleration voltage of 15 kV. The FESEM image of the SnS nanoparticles (Fig. 3(c)) confirms semi-cubical shape and its uniform size distribution (40–70 nm) that has good agreement with the laser light scattering. A

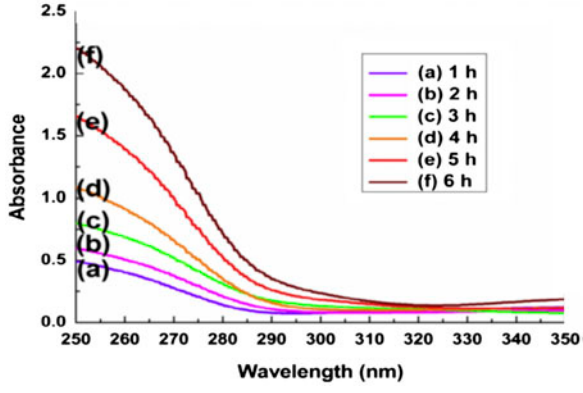

Fig. 2. Evolution of absorption spectra of the SnS nanoparticles taken at 1 h intervals following the initiation of the reaction for the first 6 h.

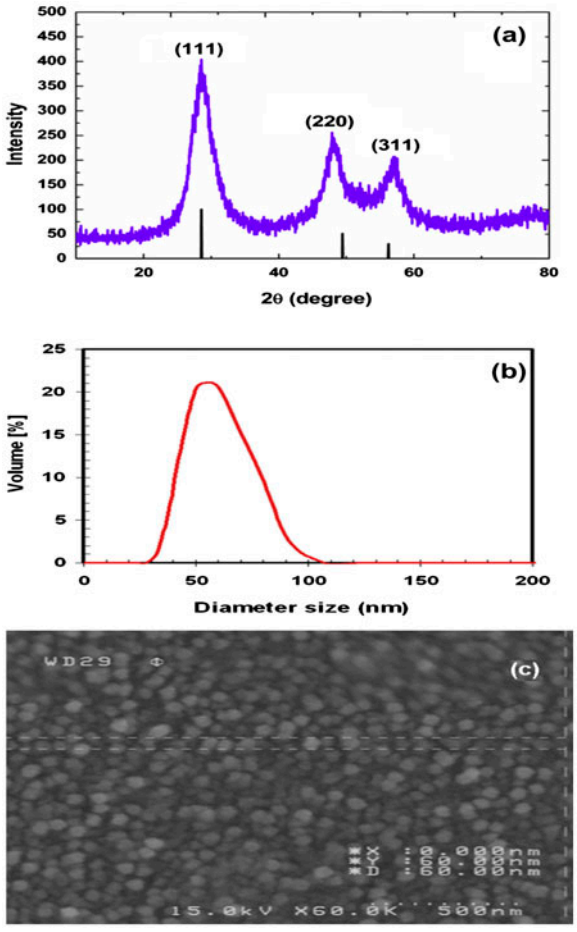

Fig. 3. (a) XRD pattern of the citrate-stabilized SnS nanoparticles; (b) histogram of the SnS nanoparticles size distribution; and (c) FESEM image of the SnS nanoparticles.

BET surface analyzer (Quantachrome NOVA 2000, USA) was used to study the surface anatomical properties i.e. surface area, total pore volume, micropore area, distribution of pore size, etc. and it also measure nitrogen adsorption–desorption isotherm at 77 K. Before each study, the samples were degassed via helium purging at 553 K for 3 h. Determination of specific surface area by N_2/77 K adsorption isotherms assumed to measure the surface area in microspores within pore sizes of a material Table 1.

3.2. Effect of pH

pH of dye solution plays a crucial role during the whole adsorption process and particularly on the adsorption capacity. For this investigation, 0.02 and 0.03 g of adsorbent was treated separately with 50 mL of CR solution (10 mg L^{-1}) at various pH values 1–6 using dilute HCl and NaOH solutions, Fig. 4 indicates that the adsorption is maximum at pH 1 hence the optimum pH for this process is 1. In acidic conditions, the surface of the adsorbent is positively charged due to the high concentration of H^+, so the electrostatic attraction between the adsorbent and the adsorbate (CR) which is an anionic dye is enhanced. Lower adsorption of CR under alkaline condition, is probably due to the presence of OH^- ions on the surface of adsorbent competing with the adsorbate (anionic dye) for adsorption sites [26]. This behavior can be explained on the basis of change in surface charge of the SnS-NP-AC. In the case of CR, an anionic dye, at higher pH, the OH^- ions compete effectively with dye anions causing a decrease in q_e. At lower pH, the surface of carbon gets positively charged, which enhances the negatively charged dye anions through electrostatic force of attraction.

3.3. Effects of contact time

The contact time significantly affect the ratio of dye molecule to vacant adsorbent active sites, the rate and amount of dye that can be transferred to the adsorbent surface. The effect of contact time on removal percentage of both dyes is shown in Fig. 5, it clearly depicts that complete and quantitative removal of dye occur in time less than 4 min for all initial dye concentration. Therefore, for subsequent work the optimum stirring time of 4 min was selected for initial concentrations of 10, 30, and 50 mg L^{-1} using 0.03 g of adsorbent. It was seen that by increasing initial dye concentration from 10 to 50 mg L^{-1} for 50 mL of 0.03 g of adsorbent, the removal percentage significantly decreased and further addition has no significant influence on their removal percentage. The great amount of dye uptake takes place in the first 2 min and equilibrium reached within 4.0 min, beyond equilibrium time, the removal percentage do not change significantly. This is mainly because of the fact that at the initial stage of adsorption, the high number of vacant surface sites and reactive sites are available, which causes the rapid adsorption of noxious dye onto the developed adsorbent. Subsequently, due to saturation of some reactive sites and possible repulsive force between adsorbed dye and bulk non-retained dye, the removal percentages significantly decrease or has slow enhance [2–4].

3.4. Effect of adsorbent dosage

The adsorbent dose shows the limit of adsorbent capacity and its ability for quantitative removal of dye for a given initial concentration [4]. The effect of

Table 1
Summary report of tin sulfide nanoparticles loaded on AC

Summary report	
Surface area	
BET surface area	1,305.12 m^2/g
Langmuir surface area	1,788.91 m^2/g
Pore volume	
Single point adsorption total pore volume of pores less than 1,256.713 Å width at $p/p^\circ = 0.985304522$	0.653 cm^3/g
Pore size	
Adsorption average pore width (4 V/A by BET)	20.04 Å
BJH adsorption average pore width (4 V/A)	36.69 Å
BJH desorption average pore width (4 V/A)	33.82 Å
Nanoparticle size	
Average particle size	45.973 Å

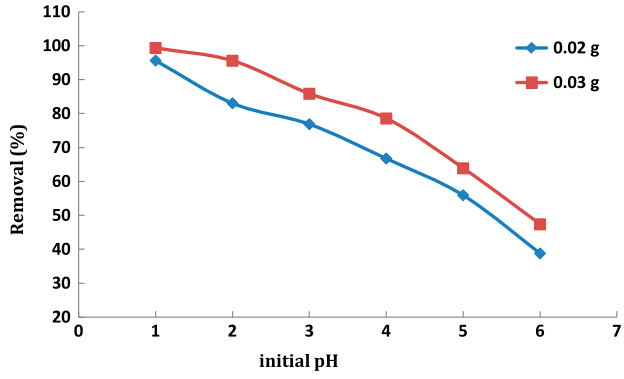

Fig. 4. Effect of system pH on adsorption of CR onto SnS-NP-AC (0.02, 0.03 g, 10 mg L^{-1}) at room temperature (27 ± 2°C), agitation speed 400 rpm for the maximum contact time required to reach the equilibrium (4 min).

adsorbent dosage (0.01–0.03 g) on the adsorption of CR (Fig. 6) from 50 mL of 5, 10, 20, 30, 40, 50, and 70 mg L^{-1} at pH 1 after 4 min shows that by raising the amount of adsorbent until 0.03 g the removal percentage increased and further addition does not significantly influence the CR removal. Rapid increase in adsorbed amount with increasing adsorbent dose is mainly concerned to greater surface area and availability of more adsorption sites. Thus, 0.03 g of adsorbent was chosen as the optimum amount of SnS-NP-AC for the quantitative removal of CR.

3.5. Effect of initial dye concentration

The experimental results for CR adsorption on both adsorbent at various concentrations (5, 10, 15, 20, 25, 30, 35, 40, 50, 60, and 70 mg L^{-1}) reveal that the removal percentage decreases with increase in the initial dye concentration, while the actual amount of

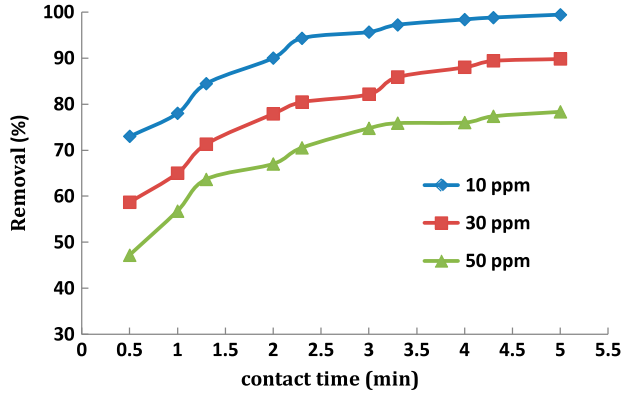

Fig. 5. Effect of contact time on CR removal at 0.03 g of SnS-NP-AC at room temperature, pH 1 and CR concentration of 10, 30, and 50 mg L^{-1}, respectively.

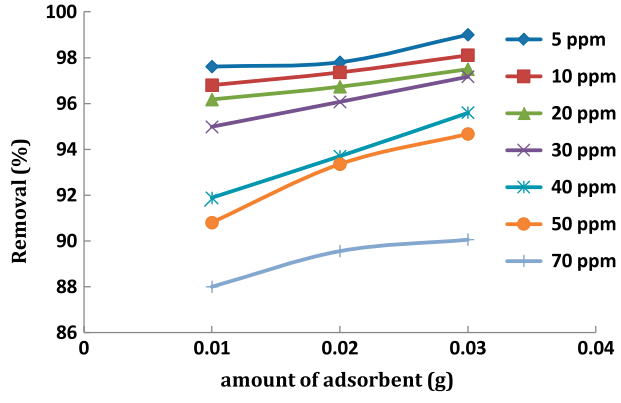

Fig. 6. Effect of adsorbent dosage and initial concentration on removal of CR at 0.02–0.04 g of SnS-NP-AC all section at 50 ml, pH 1, dye concentrations of 5–70 mg L^{-1}.

adsorbed CR per unit mass of both adsorbents increased. The result confirms high dependency of adsorption efficiency to initial CR concentration (Fig. 6). At lower CR concentration, high surface area of vacant sites of adsorbent are available that lead to increase in the concentration gradient and rate of CR diffusion to adsorbent. At high concentration of Congo red the available sites of adsorbent become fewer and hence, the CR removal percentage is dependent of initial dye concentration. The effect of initial dye concentration on the adsorption capacity of the SnS-NP-AC was investigated under equilibrium conditions with a concentration of 0.03 of both adsorbent. The increase in the CR adsorption percentage is attributed to increase in the adsorption site and the ratio of vacant site of the SnS-NP-AC to free non-adsorbed dye molecule [25,26].

3.6. RF model

RF has three tuning parameters: n_{tree}, m_{try}, and extra options. Table 2 displays the range tuning parameters and achieved coefficient of determination (R^2) and MSE for the training and testing set. As can be seen, the optimal tuning parameters for RF model are achieved based on the $n_{tree} = 100$, $m_{try} = 1$ and without extra options in the forest. In optimal model, for the training and testing sets, the MSE values of 0.0036 and 0.0073 and the R^2 values of 0.9793 and 0.9784 are achieved, respectively. Fig. 7(a) represents the predicted data vs. the experimental data. This figure displays that predicted values for training and testing sets demonstrates good agreement with experimental data. Fig. 7(b) exhibits the OOB error rate against number of trees. It can be seen that OOB error rate converges at a point after about 200 trees and remains constant, and adding more trees does not help. The importance of each variable can be represented by a mean decrease in Gini index and a mean decrease in accuracy. For the mean decrease in accuracy, a variable is evaluated in the OOB error computation. Variables with a large mean decrease in accuracy are more important among the data. The homogeneity of the nodes and leaves in the resulting

Table 2
The range of tuning parameters and obtained statistical data for training and testing data-sets

				Training set		Testing set	
	n_{tree}	m_{try}	Extra_options	R^2	MSE	R^2	MSE
1	500	1	–	0.9754	0.0047	0.9651	0.0091
2	**100**	**1**	–	**0.9793**	**0.0036**	**0.9784**	**0.0073**
3	100	2	–	0.9533	0.0023	0.9653	0.0074
4[a]	500	1	–	0.9767	0.0047	0.9660	0.0088
5[b]	100	4	Without replacement	0.9483	0.0039	0.9389	0.0031
6	100	4	Sample size = size (X_trn,1)*2/3	0.9450	0.0092	0.9597	0.0128
7[c]	100	4	Node size = 7	0.9621	0.0063	0.9720	0.0100
8[d]	100	4	Importance = 1	0.9776	0.0038	0.9762	0.0066
9[d]	100	4	Local Imp = 1	0.9759	0.0063	0.9566	0.0102
10[d]	100	4	Proximity = 1	0.9747	0.0050	0.9615	0.0083
11[e]	100	4	Proximity = 1 oob_prox = 0	0.9729	0.0037	0.9557	0.0088
12[d]	100	4	do_trace = 1	0.9721	0.0050	0.9747	0.0081
13[d]	100	4	In bag = 1	0.9754	0.0045	0.9636	0.0073
14[d]	100	2	Importance = 1 nPerm = 1	0.9748	0.0052	0.9668	0.0082
15	100	2	Importance = 1 nPerm = 3	0.9625	0.0018	0.9743	0.0063

Note: The numbers in bold indicate the best model.
[a]Set to defaults trees and m_{try} by specifying values as 0.
[b]Set sampling without replacement (default is with replacement).
[c]Note that the default value is 5 for regression.
[d]Default (Don't) = 0.
[e]Default = 1 if proximity is enabled, Don't 0.

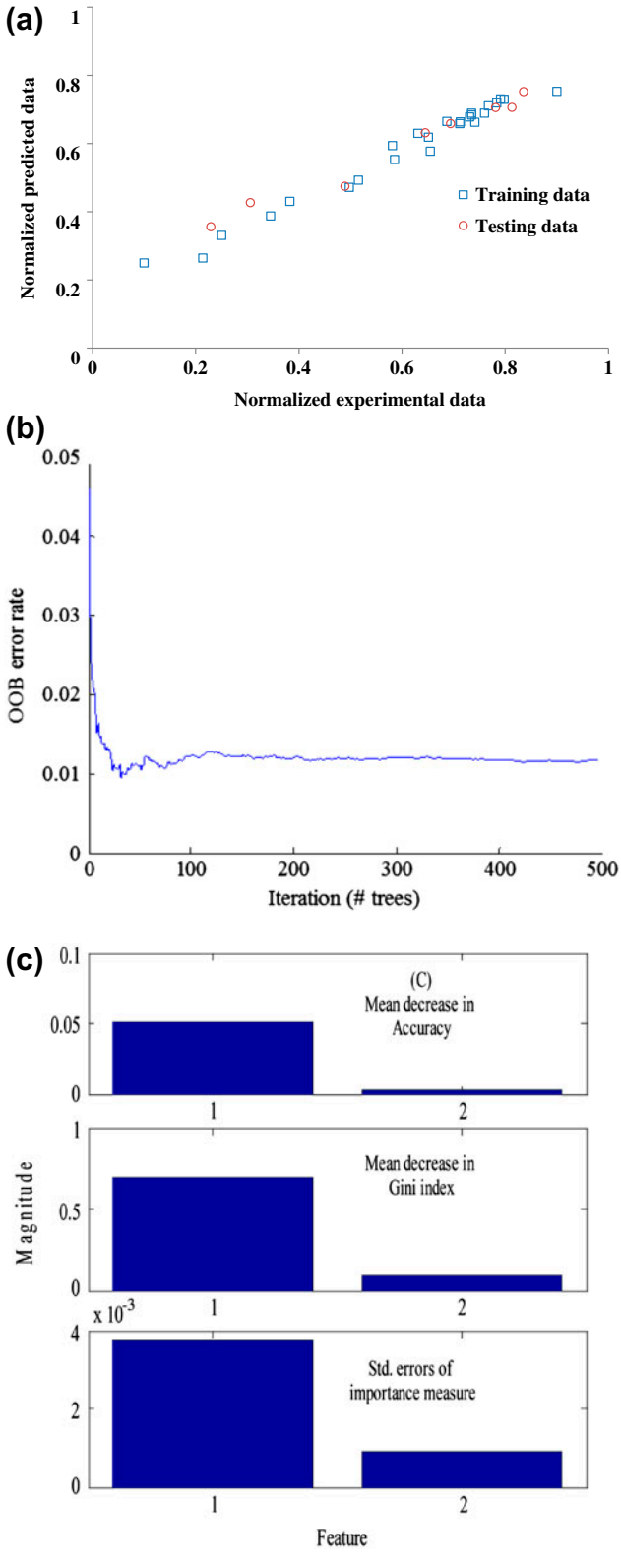

Fig. 7. (a) The experimental data vs. the predicted data, (b) the OOB error rate vs. number of trees, and (c) the importance of each parameter.

RF for each variable can be obtained by the mean decrease in Gini index. Variables with a large mean decrease in Gini index have higher purity (Fig. 7(c)).

3.7. Adsorption kinetics

Adsorption kinetics is an important characteristic regarding the determination of the adsorption process efficiency. The adsorption of a solute by a solid in aqueous solutions is a phenomenon, which usually has complex kinetics. The rate of adsorption is strongly influenced by several parameters related to the state of the adsorbent, which has heterogeneous surface in most cases, and to the physicochemical conditions under which adsorption is carried out. In order to interpret the experimental data, it is necessary to determine the step that governs the overall removal rate in the adsorption process, which is actually a sequence of steps: (1) transport of the adsorbate from the fluid to the external surface of the adsorbent across the boundary layer (film diffusion), (2) diffusion of the adsorbate within the pores of the adsorbent (particle diffusion), and (3) adsorption itself onto the surface. Out of these, the third process is considered as very fast and cannot be treated as a rate-limiting step for the uptake of the dye. For the other two steps, the following three possibilities remain: (case 1) external transport > internal transport, where rate is governed by a particle diffusion, (case 2) external transport < internal transport, where rate is governed by a film diffusion, (case 3) external transport = internal transport, the transport of adsorbate to the boundary may not be possible at a significant rate leading to the formation of a liquid film having a concentration gradient surrounding the sorbent particles [27], but the third case may be excluded [28]. Various kinetic models are available in the literature for the description of the adsorption mechanism. In this study, the pseudo-first-order model, pseudo-second-order model, Elovich equation, and intraparticle diffusion model were tested for the applicability to describe the CR adsorption process onto SnS-NP-AC. Each of the investigated models was fitted by a linear regression to the experimental data, evaluating their appropriateness on the basis of the corresponding correlation coefficients R^2. The rate constants calculated by the best fitting model were applied for the estimation of the activation parameters. The latter comprise important information that would be required in the adsorption process design for CR wastewater treatment applications. The agreement of experimental data and the model-predicted values was expressed by the correlation coefficients (R^2, values close and agreement

between experimental and equilibrium adsorption capacity). The Lagergren equation is commonly expressed as follows:

$$\log(q_e - q_t) = \log(q_e) - (K_1/2.303)t \quad (7)$$

In this model, the plot of $\log(q_e - q_t)$ vs. t may attain line that K_1 and q_e can be determined from its slope and intercept. The difference in the values of experimental and theoretical q_e reveals the in-sufficiency of this model, even when plot has high value of correlation coefficient [29]. However, the linear relation of initial solute concentration and rate of adsorption in the presence of pore diffusion fail to explain the adsorption data. The low correlation coefficient R^2 and distance of experimental and theoretical (q_e) value (Table 3), indicates the nano-applicability of this model for prediction of adsorption data. The pseudo-second-order model [30] with well-known Eq. (8) was tested to analyze and evaluate the efficiency of experimental data.

$$t/q_t = 1/K_2 q_e^2 + (1/q_e)t \quad (8)$$

In despite low correlation coefficient of plots of t/q_t vs. t and its in-applicability over the entire sorption period, the plots of t/q_t vs. t give a straight line with high correlation, which show the applicability of this model for interpretation of experimental data for all the initial dye concentrations. Values of K_2 and q_e were calculated from the intercept and slope of the plots of t/q_t vs. t, respectively (Table 3). R^2 values for pseudo-second-order kinetic model are high (0.9999) for SnS-NP-AC and the calculated q_e values are mainly close to the experimental data. This indicates that the CR—SnS-NP-AC adsorption systems obey the pseudo-second-order kinetic model for the entire sorption period. The Elovich equation is another rate equation based on the adsorption capacity is given as follows [31,32]:

$$q_t = 1/\beta \ln(\alpha\beta) + 1/\beta \ln(t) \quad (9)$$

Plot of q_t vs. $\ln(t)$ should yield a linear relationship if the Elovich is applicable with a slope of $(1/\beta)$ and an intercept of $(1/\beta)\ln(\alpha\beta)$. The Elovich constants obtained from the slope and the intercept of the straight line are reported in Table 3 [33]. Another alternative method for kinetic evaluation of an adsorption process is intraparticle diffusion [34,35]. This model is based on transport of target species from aqueous solution to the adsorbents by intraparticle diffusion according to the famous well known equation:

$$q_t = K_{diff} t^{1/2} + C \quad (10)$$

The values of K_{diff} and C were calculated from the slopes of q_t vs. $t^{1/2}$ and their values are reported in Table 3. The values of q_t were found to give two lines part with values of $t^{1/2}$ and the rate constant K_{diff} directly evaluated from the slope of the second regression line. Intraparticle diffusion is the sole rate-limiting step [36,37], when the

Table 3
Kinetic parameters of CR adsorption onto SnS-NP-AC Conditions: 0.03 g adsorbent over 10 and 50 mg L^{-1} at optima conditions of other variables

Parameter values: concentration dye (ppm)			
Models	Parameters	10	50
First-order kinetic model: $\log(q_e - q_t) = \log(q_e) - (K_1/2.303)t$	K_1	0.661	0.651
	q_e (cal)	3.1	8.05
	R^2	0.8765	0.6222
Second-order kinetic model: $t/q_t = 1/K_2 q_e^2 + (1/q_e)t$	K_2	0.455	0.144
	q_e (cal)	16.89	83.33
	R^2	0.9997	0.9999
Intraparticle diffusion: $q_t = K_{id} t^{1/2} + C$	K_{diff}	0.9574	3.494
	C	14.415	74.289
	R^2	0.9814	0.9815
Elovich: $q_t = 1/\beta \ln(\alpha\beta) + 1/\beta \ln(t)$	B	1.37	0.37
	α	20.66	29.67
	R^2	0.9592	0.9923
Experimental date	q_e(exp)	16.56	81.77

plot of q_t vs. $t^{1/2}$ passes through the origin and the value of C in this case was equal to zero. This phenomenon tells us that the intraparticle diffusion model may be the controlling factor in determining the kinetics of the process [38]. The distance of R^2 values (Table 3) from unity indicates the non-applicability of this model that rejects the rate-limiting step is the intraparticle diffusion process.

3.8. Adsorption equilibrium

Adsorption isotherms studies are preliminary step to design efficient adsorption systems that empirically is applicable to explain the equilibrium relationship between equilibrium CR concentration (adsorbent and removal in solution). The experimental equilibrium data of adsorption of CR was fitted to conventional isotherm models, such as Langmuir, Freundlich, Tempkin, and Dubinin–Radushkevich isotherms with well known assumption are presented in Table 4 for SnS-NP-AC. It was found that with adsorbent the adsorption capacity reduced.

3.8.1. Langmuir isotherm

The well known linear form of Langmuir's adsorption isotherm equation (Eq. (11)) was applied for the CR—SnS-NP-AC system [39].

$$C_e/q_e = 1/K_aQ_m + C_e/Q_m \quad (11)$$

where q_e is the number of moles of solute adsorbed per unit weight at concentration C (mol g^{-1}), C_e is the equilibrium molar concentration of the dye (mol L^{-1}), Q_m is the maximum adsorption capacity and b is the energy of adsorption. At all the temperatures, the $1/C_e$ vs. $1/q_e$ graphs give straight lines with appreciable values of the regression coefficient (R^2) close to unity, verifying the Langmuir adsorption model and ascertaining that monolayer formation is taking place during the adsorption of CR over the surface of SnS-NP-AC. On the basis of gradient and interception of these straight lines, Langmuir constant "b" and number of moles of the dye adsorbed per unit weight of the adsorbent (Q_m = 384.6 mg g^{-1}) have been evaluated and presented in Table 4. To confirm this result, the favorable or unfavorable CR adsorption onto Langmuir model was judged by calculation of the separation factor (R_L) as follow [40].

$$R_L = 1/(1 + K_aC_0) \quad (12)$$

where K_a (L mg^{-1}) is the Langmuir constant and C_0 (mg L^{-1}) is the initial concentration. The adsorption process can be determined as favorable when the R_L value lies between 0 and 1. It was found that for all adsorbent dosages and initial CR concentrations the R_L value are lower than 1, which suggest the favorable adsorption of the considered dye on the prepared adsorbent. On the other hand, increase in R_L value with rising initial CR concentration and adsorbent dosage show high tendency of CR for adsorption onto SnS-NP-AC.

3.8.2. Freundlich isotherm

The Freundlich model for the adsorption of solutes from a liquid to a solid surface was applied for the present adsorption system [41]:

$$\ln q_e = \ln K_F + (1/n) \ln C_e \quad (13)$$

where q_e is the amount adsorbed (mol g^{-1}), C_e is the equilibrium concentration of the adsorbate (CR), K_F and n the Freundlich constants, are related to adsorption capacity and adsorption intensity, respectively. Straight lines with regression coefficients close to unity were obtained in ln C_e vs. ln q_e, graph and values of constants K_F and n derived from the intercepts and slope of these straight lines are presented in Table 4. The verification of the Freundlich model confirms the homogeneous nature of adsorption of CR over the surface of SnS-NP-AC at each temperature.

3.8.3. Temkin isotherm

The Temkin isotherm Eq. (14) can be simplified to the following equation [42]:

$$q_e = B_1 \ln K_T + B_1 \ln C_e \quad (14)$$

where $B_1 = (RT)/b$ is related to the heat of adsorption, T is the absolute temperature in Kelvin and R is the universal gas constant, 8.314 (J mol^{-1} K^{-1}). The adsorption data were analyzed according to the linear form of the Temkin isotherm Eq. (14). Examination of the data shows that the Temkin isotherm is efficiently applicable for fitting the CR adsorption onto SnS-NP-AC. The linear isotherm constants and coefficients of determination are presented in Table 4. The heat of CR adsorption onto SnS-NP-AC was found to increase from 2.236 to 2.500 kJ mol^{-1} with increase in SnS-NP-

Table 4
Isotherm constant parameters and correlation coefficients calculated for the adsorption at various concentration of CR (5–70 mg L^{-1}) onto SnS-NP-AC

Adsorbent (g)				
Isotherm	Parameters	0.01	0.02	0.03
Langmuir: $C_e/q_e = 1/K_aQ_m + C_e/Q_m$	Q_m (mg g^{-1})	384.61	188.67	126.58
	K_a (L mg^{-1})	0.393	0.525	0.693
	R_L	0.048–0.337	0.026–0.276	0.020–0.223
	R^2	0.9751	0.9858	0.9963
Freundlich: ln q_e = ln K_F + (1/n)ln C_e	1/n	0.6099	0.595	0.522
	K_F (L mg^{-1})	96.69	56.689	45.98
	R^2	0.9551	0.9726	0.962
Temkin: $q_e = B_1$ ln $K_T + B_1$ lnC_e	B_1	72.126	35.345	26.096
	K_T (L mg^{-1})	53.48	108.93	111.18
	R^2	0.9653	0.9578	0.9876
Dubinin and Radushkevich: Ln q_e = ln $Q_s - K\varepsilon^2$	Q_s (mg g^{-1})	199.63	97.73	76.60
	K	−1E−07	−7E−08	−8E−08
	E (J/mol)= 1/(2 K)$^{1/2}$	2,236.07	2,672.6	2,500.0
	R^2	0.8947	0.8556	0.8809

Table 5
Comparison of adsorption capacities various adsorbents for Congo red dye

Dye	Adsorbent	Adsorption capacity (mg g^{-1})	Source
CR	Ni-ZnS-NP-AC	285.7	[22]
CR	Pd-NP-AC	76.92	[48]
CR	Ag-NP-AC	66.67	[48]
CR	ZnO-NP-AC	142.86	[48]
CR	AC-Coir Pith	6.72	[49]
CR	AC-BFA	1.867	[50]
CR	KJA-Ti	52	[51]
CR	KJA/S/CaFe	159	[51]
CR	KJA/N/CaFe	161	[51]
CR	SA/N/CaFe	189	[51]
CR	CAC	300	[52]
CR	SnS-NP-AC	384.6	Present work

AC dosage from 0.01 to 0.03 g. The correlation coefficients R^2 obtained from Temkin model were comparable to that obtained for Langmuir and Freundlich equations, which explain the applicability of Temkin model to the adsorption of CR onto SnS-NP-AC.

3.8.4. Dubinin–Radushkevich isotherm

In order to identify nature of the ongoing adsorption process, following D–R adsorption isotherm model was applied [43,44]:

$$\ln q_e = \ln Q_s - K\varepsilon^2 \quad (15)$$

where q_e is the amount of the dye adsorbed per unit weight of the adsorbent (mg g^{-1}), Q_s is the maximum sorption capacity provided by the intercept (μmol g^{-1}), K ($mol^2\ J^{-2}$) is the activity coefficient related to mean sorption energy, and ε (Eq. (16)) is Polanyi potential [45].

$$\varepsilon = RT\ \ln(1 + 1/C_e) \quad (16)$$

where R is universal gas constant and T is temperature in Kelvin. The activity coefficient (K) and the adsorption capacities (ln Q_s) were evaluated from the slopes and intercepts of the plot ln q_e vs. ε^2 at 25°C and these results are depicted in Table 4. The mean sorption energy (E) was calculated from the values of K by following expression [45–47]:

$$E = 1/\sqrt{2K} \quad (17)$$

On the basis of values of K, obtained from the D–R isotherm graph, values of mean sorption energy were calculated at each temperature.

3.9. Comparison with other adsorbents

This study was compared to the previously studied research of the considered dye i.e. CR using different adsorbent (Table 5). It is seen that when, SnS nanoparticle loaded on AC, it lead to rapid decrease in contact time parameter, it is reported that time taken by AC is about 240 min [50], but when AC loaded with SnS nanoparticle time taken by the adsorbent rapidly decrease and it takes nearly 4 min to adsorb the maximum amount of Congo red. Secondly, the maximum amount of the adsorbate adsorbed on the adsorbent also increases form 1.867 mg/g (for AC) it becomes 384.6 mg/g (for SnS nanoparticles loaded on AC). It was clearly depicted from the table that the developed adsorbent has the maximum adsorption capacity in comparison to the previously developed adsorbent for the same dye removal [22,48–52].

4. Conclusion

In this work, the RF model has been used as power approach for predicting the CR adsorption on to the tin Sulfide nanoparticles loaded on AC. The results clearly depicts that there is a good agreement between experimental data and predicted data using the RF model. Tin Sulfide nanoparticles were synthesized and loaded on AC prepared by walnut crust and which were further characterized using analytical techniques such as SEM, BET, XRD, and UV–Vis spectroscopy. The developed adsorbent was used for the removal of CR in a batch sorption process and the influence of parameters such as initial dye concentration (15 mg L^{-1}), contact time (4 min), initial pH (pH 1), and the amount of adsorbent (0.03 g) on CR removal was investigated. The experimental data were analyzed by the Langmuir, Freundlich, Tempkin, and Dubinin–Radushkevich isotherm models and the

results showed that the experimental equilibrium data was best fitted and described by the Langmuir isotherm model. The adsorption kinetics data of CR adsorption onto SnS-NP-AC was found to be in good agreement with the pseudo-second-order model and intraparticle diffusion model. The SnS-NP-AC is applicable for quantity removal of CR for a contact time of 4 min with adsorption capacity of 384.6 mg g^{-1}. On the other hand, the experimental results showed that SnS-NP-AC can be used at least for four times without any considerable change in its adsorption properties. By considering all of these results, it can be concluded that SnS-NP-AC can be utilized as a new and effective adsorbent in the removal of CR, a highly toxic dye, from waters and wastewaters.

References

[1] A. Ghaedi, A. Vafaei, M. Mohagheghian, N. Afshar, S. Hafezi, Fuzzy modelling of concentration in chamomile solution using reverse osmosis, Fresenius Environ. Bull. 21 (2012) 634–643.

[2] M. Ghaedi, A.M. Ghaedi, E. Negintaji, A. Ansari, A. Vafaei, M. Rajabi, Random forest model for removal of bromophenol blue using activated carbon obtained from Astragalus bisulcatus tree, J. Ind. Eng. Chem. 20 (2014) 1793–1803.

[3] M. Ghaedi, A. Ansari, F. Bahari, A. Ghaedi, A. Vafaei, A hybrid artificial neural network and particle swarm optimization for prediction of removal of hazardous dye brilliant green from aqueous solution using zinc sulfide nanoparticle loaded on activated carbon, Spectrochim. Acta A: Mol. Biomol. Spectrosc. 137 (2015) 1004–1015.

[4] M. Ghaedi, A. Ghaedi, A. Ansari, F. Mohammadi, A. Vafaei, Artificial neural network and particle swarm optimization for removal of methyl orange by gold nanoparticles loaded on activated carbon and Tamarisk, Spectrochim. Acta A: Mol. Biomol. Spectrosc. 132 (2014) 639–654.

[5] M. Ghaedi, A.M. Ghaedi, F. Abdi, M. Roosta, A. Vafaei, A. Asghari, Principal component analysis-adaptive neuro-fuzzy inference system modeling and genetic algorithm optimization of adsorption of methylene blue by activated carbon derived from Pistacia khinjuk, Ecotoxicol. Environ. Saf. 96 (2013) 110–117.

[6] M. Ghaedi, A.M. Ghaedi, E. Negintaji, A. Ansari, F. Mohammadi, Artificial neural network—Imperialist competitive algorithm based optimization for removal of sunset yellow using $Zn(OH)_2$ nanoparticles-activated carbon, J. Ind. Eng. Chem. 20 (2014) 4332–4343.

[7] M. Ghaedi, R. Hosaininia, A. Ghaedi, A. Vafaei, F. Taghizadeh, Adaptive neuro-fuzzy inference system model for adsorption of 1,3,4-thiadiazole-2,5-dithiol onto gold nanoparticales-activated carbon, Spectrochim. Acta A: Mol. Biomol. Spectrosc. 131 (2014) 606–614.

[8] M. Ghaedi, N. Zeinali, A.M. Ghaedi, M. Teimuori, J. Tashkhourian, Artificial neural network-genetic algorithm based optimization for the adsorption of methylene blue and brilliant green from aqueous solution by graphite oxide nanoparticle, Spectrochim. Acta. A: Mol. Biomol. Spectrosc. 125 (2014) 264–277.

[9] S. Hajati, M. Ghaedi, H. Mazaheri, Removal of methylene blue from aqueous solution by walnut carbon: optimization using response surface methodology, Desalin. Water Treat. 52 (2014) 1–15.

[10] M. Ghaedi, S. Hajjati, Z. Mahmudi, I. Tyagi, S. Agarwal, A. Maity, V.K. Gupta, Modeling of competitive ultrasonic assisted removal of the dyes—Methylene blue and Safranin-O using Fe_3O_4 nanoparticles, Chem. Eng. J. 268 (2015) 28–37.

[11] N. Goudarzi, D. Shahsavani, F. Emadi-Gandaghi, M.A. Chamjangali, Application of random forests method to predict the retention indices of some polycyclic aromatic hydrocarbons, J. Chromatogr. A 1333 (2014) 25–31.

[12] A. Acharjee, B. Kloosterman, R.C. de Vos, J.S. Werij, C.W. Bachem, R.G. Visser, C. Maliepaard, Data integration and network reconstruction with ~omics data using Random Forest regression in potato, Anal. Chim. Acta. 705 (2011) 56–63.

[13] F. Nekouei, S. Nekouei, I. Tyagi, V.K. Gupta, Kinetic, thermodynamic and isotherm studies for acid blue 129 removal from liquids using copper oxide nanoparticle-modified activated carbon as a novel adsorbent, J. Mol. Liq. 201 (2015) 124–133.

[14] H. Mahmoodian, O. Moradi, B. Shariatzadeha, T.A. Saleh, I. Tyagi, A. Maity, M. Asif, V.K. Gupta, Enhanced removal of methyl orange from aqueous solutions by poly HEMA–chitosan-MWCNT nanocomposite, J. Mol. Liq. 202 (2014) 189–198.

[15] M.H. Schwartz, A. Rozumalski, W. Truong, T.F. Novacheck, Predicting the outcome of intramuscular psoas lengthening in children with cerebral palsy using preoperative gait data and the random forest algorithm, Gait Posture 37 (2013) 473–479.

[16] C.M. Kao, M.S. Chou, W.L. Fang, B.W. Liu, B.R. Huang, Regulating colored textile wastewater by 3/31 wavelength admi methods in Taiwan, Chemosphere 44 (2001) 1055–1063.

[17] P.J.M. Carrott, Suhas, M.M.L. Ribeiro Carrott, C.I. Guerrero, L.A. Delgado, Reactivity and porosity development during pyrolysis and physical activation in CO_2 or steam of kraft and hydrolytic lignins, J. Anal. Appl. Pyrolysis 82 (2008) 264–271.

[18] M. Ghaedi, F. Karimi, B. Barazesh, R. Sahraei, A. Daneshfar, Removal of Reactive Orange 12 from aqueous solutions by adsorption on tin sulfide nanoparticle loaded on activated carbon, J. Ind. Eng. Chem. 19 (2013) 756–763.

[19] M. Roosta, M. Ghaedi, A. Daneshfar, R. Sahraei, Experimental design based response surface methodology optimization of ultrasonic assisted adsorption of safaranin O by tin sulfide nanoparticle loaded on activated carbon, Spectrochim. Acta A: Mol. Biomol. Spectrosc. 122 (2014) 223–231.

[20] M. Ravanan, M. Ghaedi, A. Ansari, F. Taghizadeh, D. Elhamifar, Comparison of the efficiency of Cu and silver nanoparticle loaded on supports for the removal of Eosin Y from aqueous solution: Kinetic and isotherm study, Spectrochim. Acta A: Mol. Biomol. Spectrosc. 123 (2014) 467–472.

[21] M. Ghaedi, A. Ansari, M.H. Habibi, A.R. Asghari, Removal of malachite green from aqueous solution by zinc oxide nanoparticle loaded on activated carbon: Kinetics and isotherm study, J. Ind. Eng. Chem. 20 (1) (2014) 17–28.

[22] K. Ahmadi, M. Ghaedi, A. Ansari, Comparison of nickel doped Zinc Sulfide and/or palladium nanoparticle loaded on activated carbon as efficient adsorbents for kinetic and equilibrium study of removal of Congo Red dye, Spectrochim. Acta A: Mol. Biomol. Spectrosc. 136 (2015) 1441–1449.
[23] L. Breiman, M. Lear, Random forests, Mach. Learn. 45 (2001) 5–32.
[24] Suhas, P.J.M. Carrott, M.M.L. Ribeiro Carrott, Using alkali metals to control reactivity and porosity during physical activation of demineralised kraft lignin, Carbon 47 (2009) 1012–1017.
[25] X. Xu, J. Zhuang, X. Wang, SnO_2 quantum dots and quantum wires: Controllable synthesis, self-assembled 2D architectures, and gas-sensing properties, J. Am. Chem. Soc. 130 (2008) 12527–12535.
[26] A. Mittal, V.K. Gupta, A. Malviya, J. Mittal, Process development for the batch and bulk removal and recovery of a hazardous, water-soluble azo dye (Metanil Yellow) by adsorption over waste materials (Bottom Ash and De-Oiled Soya), J. Hazard. Mater. 151 (2008) 821–832.
[27] A. Mittal, J. Mittal, L. Kurup, A.K. Singh, Process development for the removal and recovery of hazardous dye erythrosine from wastewater by waste materials—Bottom Ash and De-Oiled Soya as adsorbents, J. Hazard. Mater. 138 (2006) 95–105.
[28] C.Y.Flores, C. Diaz, A. Rubert, G.A. Benítez, M.S. Moreno, M.A. Fernández Lorenzo de Mele, R.C. Salvarezza, P.L. Schilardi, C. Vericat, Spontaneous adsorption of silver nanoparticles on Ti/TiO_2 surfaces. Antibacterial effect on *Pseudomonas aeruginosa*, J. Colloid Interface Sci. 350 (2010) 402–408.
[29] Y.S. Ho, G. McKay, D.A.J. Wase, C.F. Forster, Study of the sorption of divalent metal ions on to peat, Adsorpt. Sci. Technol. 18 (2000) 639–650.
[30] Y.S. Ho, Adsorption of Heavy Metals from Waste Streams by Peat, Ph.D. Thesis, The University of Birmingham, Birmingham, 1995.
[31] Y.S. Ho, D.A.J. Wase, C.F. Forster, Kinetic studies of competitive heavy metal adsorption by sphagnum moss peat, Environ. Technol. 17 (1996) 71–77.
[32] Y.S. Ho, Second-order kinetic model for the sorption of cadmium onto tree fern: A comparison of linear and non-linear methods, Water Res. 40 (2006) 119–125.
[33] A. Khaled, A. El Nemr, A. El-Sikaily, O. Abdelwahab, Removal of direct N Blue-106 from artificial textile dye effluent using activated carbon from orange peel: Adsorption isotherm and kinetic studies, J. Hazard. Mater. 165 (2009) 100–110.
[34] G. McKay, The adsorption of dyestuff from aqueous solution using activated carbon: Analytical solution for batch adsorption base donexternal mass transfer and pore diffusion, Chem. Eng. J. 27 (1983) 187–196.
[35] J. Acharya, J.N. Sahu, B.K. Sahoo, C.R. Mohanty, B.C. Meikap, Removal of chromium(VI) from wastewater by activated carbon developed from Tamarind wood activated with zinc chloride, Chem. Eng. J. 150 (2009) 25–39.
[36] G. Crini, H.N. Peindy, F. Gimbert, C. Robert, Removal of C.I. Basic Green 4 (Malachite Green) from aqueous solutions by adsorption using cyclodextrin-based adsorbent: Kinetic and equilibrium studies, Sep. Purif. Technol. 53 (2007) 97–110.
[37] Alok Mittal, Jyoti Mittal, Arti Malviya, V.K. Gupta, Adsorptive removal of hazardous anionic dye "Congo red" from wastewater using waste materials and recovery by desorption, J. Colloid Interface Sci. 340 (2009) 16–26.
[38] V.K. Gupta, S. Khamparia, I. Tyagi, D. Jaspal, A. Malviya, Decolorization of mixture of dyes: A critical review, Global J. Environ. Sci. Manage. 1 (2015) 71–94.
[39] I. Langmuir The adsorption of gases on plane surfaces of glass, mica and platinum, J. Am. Chem. Soc. 40 (1918) 1361–1403.
[40] A. Shamsizadeh, M. Ghaedi, A. Ansari, S. Azizian, M.K. Purkait, Tin oxide nanoparticle loaded on activated carbon as new adsorbent for efficient removal of malachite green-oxalate: Non-linear kinetics and isotherm study, J. Mol. Liq. 195 (2014) 212–218.
[41] H.M.F. Freundlich, Uber die adsorption in losungen (Over the adsorption in solution), Z. Phys. Chem. 57 (1906) 385–470.
[42] M.J. Temkin, V. Pyzhev, Recent modifications to Langmuir isotherms, Acta Physiochim. USSR 12 (1940) 217–222.
[43] M.M. Dubinin, The potential theory of adsorption of gases and vapors for adsorbents with energetically non-uniform surface, Chem. Res. 60 (1960) 235–266.
[44] M.M. Dubinin, Modern state of the theory of volume filling of micropore adsorbents during adsorption of gases and steams on carbon adsorbent, Zh. Fiz. Khim. 39 (1965) 1305–1317.
[45] L.V. Radushkevich, Potential theory of sorption and structure of carbons, Zh. Fiz. Khim. 23 (1949) 1410–1420.
[46] V.K. Gupta, Suhas, A. Nayak, S. Agarwal, M. Chaudhary, I. Tyagi, Removal of Ni (II) ions from water using scrap tire, J. Mol. Liq. 190 (2014) 215–222.
[47] V.K. Gupta, I. Ali, Suhas, D. Mohan, Equilibrium uptake and sorption dynamics for the removal of a basic dye (basic red) using low-cost adsorbents, J. Colloid Interface Sci. 265 (2003) 257–264.
[48] M. Ghaedi, M. Nejati Biyareh, S. Nasiri Kokhdan, S.H. Shamsaldini, R. Sahraei, A. Daneshfar, S. Shahriyar, Comparison of the efficiency of palladium and silver nanoparticles loaded on activated carbon and zinc oxide nanorods loaded on activated carbon as new adsorbents for removal of Congo red from aqueous solution: Kinetic and isotherm study, Mater. Sci. Eng., C 32 (2012) 725–734.
[49] C. Namasivayam, D. Kavitha, Removal of Congo Red from water by adsorption onto activated carbon prepared from coir pith, an agricultural solid waste, Dyes Pigm. 54(1) (2002) 47–58.
[50] I.D. Mall, V.C. Srivastava, N.K. Agarwal, Removal of congo red from aqueous solution by bagasse fly ash and activated carbon: Kinetic study and equilibrium isotherm analyses, Chemosphere 61 (2005) 492–501.
[51] Ewa Lorenc-Grabowska, Grażyna Gryglewicz, Adsorption characteristics of Congo Red on coal-based mesoporous activated carbon, Dyes Pigm. 74 (2007) 34–40.
[52] M.K. Purkait, A. Maiti, S. DasGupta, S. De, Removal of congo red using activated carbon and its regeneration, J. Hazard. Mater. 145 (2007) 287–295.